Electronic Supplementary Material (ESI) for Nanoscale.

SUPPORTING INFORMATION

Ionic Flash NanoPrecipitation (iFNP) for the Facile, One-Step Synthesis of Inorganic-Organic Hybrid Nanoparticles in Water

Nathalie M Pinkerton,[a] Leah Behar,[b] Khadidja Hadri,[a,c] Baptiste Amouroux,[c] Chistophe Mingotaud,[c] Daniel R. Talham,[d] Stefan Chassaing,[a]* & Jean-Daniel Marty [c]*

[a] ITAV, Université de Toulouse, CNRS USR3505, UPS
1 place Pierre Potier, 31106 Toulouse Cedex 1 (France)
**stefan.chassaing@itav.fr*

[b] Department of Chemistry, Mars Hill University
Mars Hill, NC 28754 (United States)

[c] IMRCP, Université de Toulouse, CNRS UMR5623, UPS
118 route de Narbonne, 31062 Toulouse Cedex 1 (France)
**marty@chimie.ups-tlse.fr*

[d] Department of Chemistry, University of Florida
Gainesville, Florida 32611 (United States)

Contents:

Acronyms:

BCP	**B**lock **C**o**P**olymer
DLS	**D**ynamic **L**ight **S**cattering
DMEM	**D**ulbecco's **M**odified **E**agle's **M**edium
Eu	**Eu**ropium
ICG	**I**ndo**C**yanine **G**reen
ICP	**I**nductively **C**oupled **P**lasma
iFNP	**i**onic **F**lash **N**ano**P**recipitation
FNP	**F**lash **N**ano**P**recipitation
Gd	**G**a**d**olinium
MR	**M**agnetic **R**esonance
MRI	**M**agnetic **R**esonance **I**maging
NMR	**N**uclear **M**agnetic **R**esonance
NP	**N**ano**P**article
PAA	**P**oly(**A**crylic **A**cid*)*
PAA-PEG	**P**oly(**A**crylic **A**cid*)-b-***P**oly(**E**thylene **G**lycol)
PBS	**P**hosphate **B**uffered **S**aline
PS-PEG	**P**oly(**S**tyrene)-*b*- **P**oly(**E**thylene **G**lycol)
PEG-PPO-PEG	**P**oly(**E**thylene **G**lycol)-*b*-**P**oly(**P**ropylene **O**xide)-*b*- **P**oly(**E**thylene **G**lycol)
TEM	**T**ransmission **E**lectron **M**icroscopy
XRD	**X-R**ay **D**iffraction
ZP	**Z**eta **P**otential

Materials and Experimental Procedures

Materials

PAA_{3k}-*b*-PEG_{6k}, PAA_{6k}-*b*-PEG_{11k}, $PAA_{6,5k}$-*b*-PEG_{6k} $PAA_{17,5k}$-*b*-PEG_{6k}, PAA_{56k}-*b*-PEG_{5k}, $PAA_{7,5k}$-*b*-$PEG_{22,5k}$ and $PS_{1.6k}$-PEG_{5k} were purchased from Polymer Source, Inc. Sodium chloride, sodium phosphate monobasic, sodium hydroxide, hydrochloric acid, Tris buffer, Pluronic® F-127, and gadolinium (III) nitrate hexahydrate, and indocyanine green (ICG) were purchased from Sigma-Aldrich. Bovine serum albumin was purchased from Euromedex. Europium (III) chloride hexahydrate was purchased from Alfa Aesar. DMEM media, penicillin, streptomycin, 10 mM phosphate buffered saline (PBS) and fetal bovine serum were purchased from Life Technologies. HeLa cells were purchased from ATCC. Ultra-pure water (18.2 MΩ·cm) was generated using a ELGA Purelab® Ultra purification system. PAA-PEG solutions were titrated to a pH of 5.2 using 2M NaOH. All aqueous solutions were filtered with a 0.22 µm regenerated cellulose syringe filter (Agela Technologies) to remove dust prior to use.

Nanoprobe Formation

Nanoprobes were formed *via* ionic Flash NanoPreciptation (*iFNP*) using a confined impinging jet (CIJ) mixer designed by Han *et al.*[1] As an example formulation, water stream 1 containing 10 mg/ml PAA-*b*-PEG 3k-*b*-6k and 1 mg/mL NaH_2PO_4 was rapidly mixed against water stream 2 containing 5.2 mg/mL $Gd(NO_3)_3$ using the CIJ mixer. Particles were dialyzed against ultra-pure water or 0.9 % wt/vol saline solution using a Spectra/Por® regenerated cellulose membrane (MWCO 6-8 kD).

Nanoprobe Characterization

NP size was determined *via* DLS using a Zetasizer Nano-ZS (Malvern Instruments, France). The reported particle size is the intensity weighted diameter determined by the Malvern deconvolution software in normal mode. ZP measurements were done on NPs in a 3 mM NaCl solution using the aforementioned Zetasizer Nano-ZS. TEM samples deposited on holey carbon grids and imaged on a Hitachi HT-7700. TEM images were analyzed with ImageJ. XRD samples were dialyzed against ultra-pure water using a Spectra/Por® regenerated cellulose membrane (MWCO 6-8 kD) and then lyophilized (Christ Alpha 2-4 LD lyophilizer, Germany). Powder XRD spectra of the dried powders were recorded on an MPDPro diffractometer (PANalytical B.V.) (Cu Kα source) from 2° to

90° (2θ) with a step size of 0.017°. Steady state absorption and emission spectra were made using a Xenius Fluorometer (SAFAS, Monaco) and a Fluoroskan Ascent Microplate Fluorometer (Thermo Fisher, France). Prior to ICP measurements, nanoprobe samples were digested in nitric acid for a minimum of 1 day, and then analyzed using a Perkin Elmer Optima 3200 RL (USA). MR relaxation time measurements were carried out at 1.4 T on a Minispec mq60 TD-NMR contrast agent analyzer (Bruker Optics, Billerica, MA, USA) at a constant temperature of 37 °C. T_1 relaxation times were measured using an inversion recovery pulse sequence (t1_ir_mb). T_2 relaxation times were measured using a Carr–Purcell–Meiboom–Gill pulse sequence (t2_cp_mb).

Cell Culture and Imaging

HeLa cells were cultured in DMEM media containing 10% fetal bovine serum, and 1% of penicillin/streptomycin at 37 °C with 5% CO_2 in a humid environment. Cells were incubated with a solution of 0.5 mg/mL $GdPO_4$-ICG NPs in DMEM media with 5% fetal bovine serum and 1% of penicillin/streptomycin for 3 hours. The cells were subsequently washed three times with PBS and reincubated in DMEM media prior to imaging. All imaging was performed on a Zeiss LSM 510 NLO microscope equipped a femto-second pulsed Chameleon laser from Coherent. Samples were excited at 750 nm.

Nanoprobe Stability Testing

The stability of the nanoprobes overtime under storage and physiological conditions was tested. Particles were stored at 4°C in the dark post *iFNP* formation. Their stability was monitored over the course of six days visually and *via* DLS. For biologically relevant conditions, particles were incubated in Tris buffer (pH 7.4) with 3 wt% albumin and periodically monitored visually and *via* DLS over the course of 24 hours. To distinguish both the albumin (6 to 7 nm) and the NP populations (40 nm), the intensity weighted diameters were determined by the Malvern deconvolution software in high resolution mode (multiple narrow modes).

Choice of stabilizing block copolymer

As mentioned in the main text, the choice of stabilizing polymer plays an integral role in determining the particle stability, biocompatibility and fate *in vivo*.[2] As such, we focused on PEG containing polymers: PS-PEG, PEG-PPO-PEG and PAA-PEG. In the case of both PS-PEG and PEG-PPO-PEG, the hydrophobic blocks are poorly soluble in water and necessitated the use of the water miscible, organic solvent, THF. $Gd(NO_3)_3$ is soluble in THF and was thus included in the organic stream, while the NaH_2PO_4 was kept in the aqueous stream. In the case of the PAA-PEG, the polymer was included in the aqueous stream to prevent interactions between the PAA and Gd^{3+} prior to *iFNP*. For both PS-PEG and PEG-PPO-PEG, macro-precipitates were observed after *iFNP* indicating a poor interaction between the hydrophobic blocks and the charged surface of the growing $GdPO_4$ core (Figure S1a). Conversely, the PAA-PEG formulation resulted in a clear solution of 150 nm $GdPO_4$ NPs (Figures S1a-b). The good affinity of the polyanion for the $GdPO_4$ surface is unsurprising. Anionic PAA is known to complex Gd(III) ions. The importance of the ionic interactions between PAA and the $GdPO_4$ is explored in the following section.

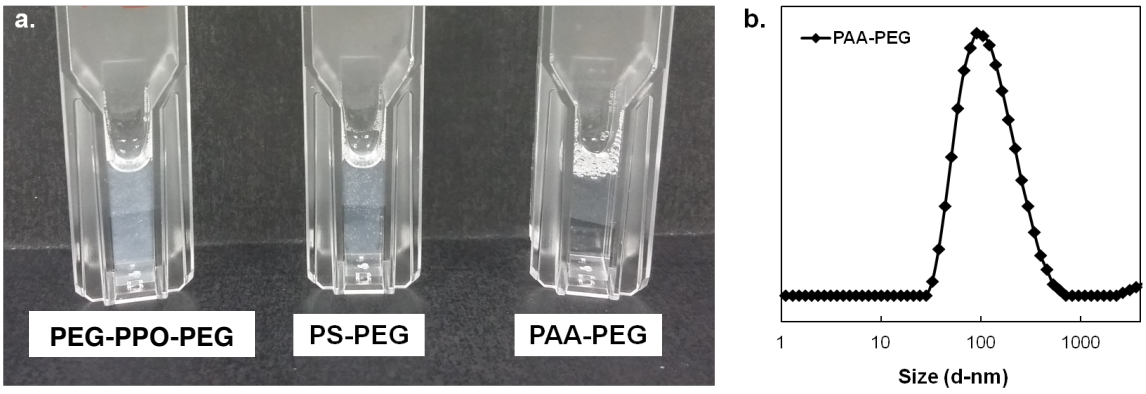

Figure S1. *(a) Images of the solutions after iFNP using PEG-PPO-PEG, PS-PEG and PAA-PEG. Large aggregates are observed in the case of PEG-PPO-PEG and PS-PEG indicating that these polymers are not suitable for stabilizing $GdPO_4$ nanoparticles. A clear solution of 150 nm nanoparticles is observed in the case of PAA-PEG. (b) The intensity weighted size distribution of the as-synthesized 150 nm PAA-PEG stabilized $GdPO_4$ nanoparticles.*

Interaction between PAA block and inorganic core

To demonstrate the importance of the ionic interaction between the acrylic acid residues of the PAA and the Gd(III) ions, a pH study was performed. We expect that at pH's one or two units below the pK_a of PAA (pK_a = 4.5),[3] the polymer is not able to interact in an ionic manner because the acrylic acids are protonated and neutral. Thus the polymer is unable to anchor strongly to the NP surface and stabilize the NPs. Conversely, at pH's at or above the pK_a of PAA, the polymer is able to interact in an ionic manner and stabilize the NPs, because a portion of the acrylic acids are deprotonated and negatively charged. Accordingly, the starting solution pHs were varied from 1 to 7 and the ability for the system to form stable NPs was determined. At pH 1, macro-precipitates were observed after *iFNP* indicating a poor interaction between the PAA and the $GdPO_4$ surface. At pH 3, 40 nm particles were formed, while at pH's 5 and 7, the system formed 30 nm NPs (Figure S2). This suggests that at pH > 3, there are a sufficient number of deprotonated carboxylic acid groups for stabilization of the particles.

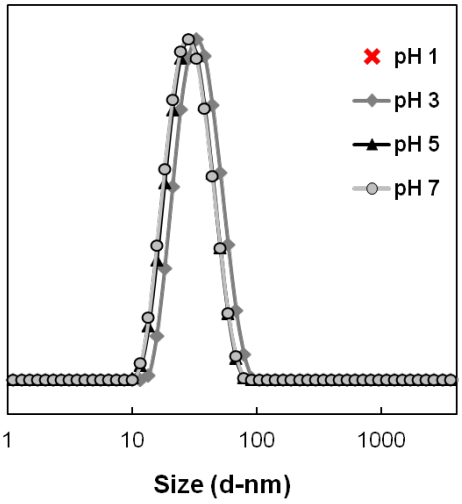

Figure S2. *The resulting NP sizes are plotted as a function of solution pH.*

Effect of the PEG-PAA structure on NP hydrodynamic diameter

Considering both distribution profiles below, $GdPO_4$ NPs with large and poorly controlled hydrodynamic diameter were obtained with polymers containing PAA unit blocks larger than PEG units or when polymers present high average molecular weights ($PAA_{17,5k}$-*b*-

PEG_{6k}, PAA_{56k}-*b*-PEG_{5k} or $PAA_{7,5k}$-*b*-$PEG_{22,5k}$). Best results were obtained with PAA_{3k}-*b*-PEG_{6k}.

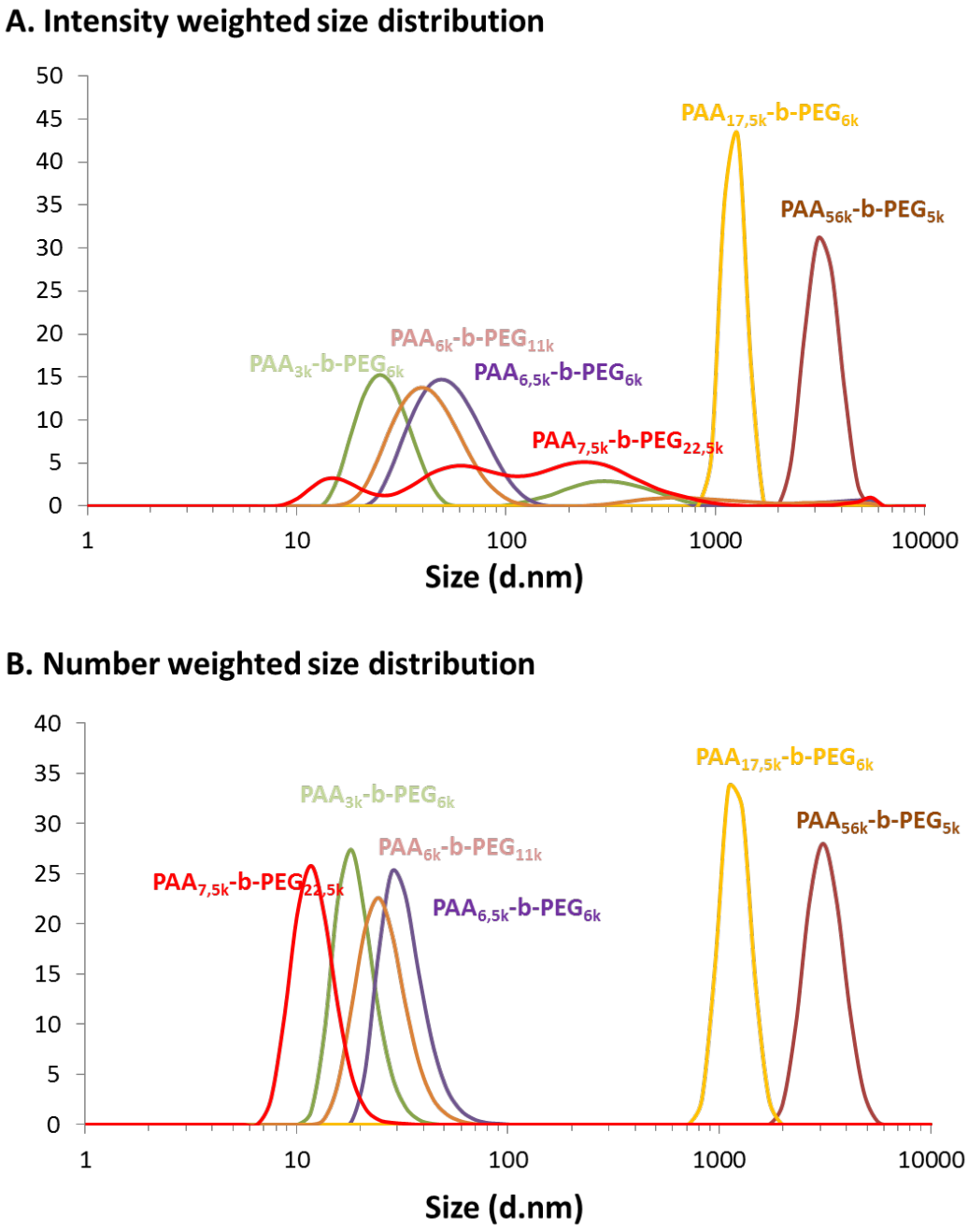

Figure S3. *Intensity and number weighted particle size distribution of $GdPO_4$ NPs obtained by using PAA-b-PEG block copolymers of different average molecular weights and compositions. Gd^{3+}/PO_4^{3-} and Gd^{3+}/[AA unit] ratio are arbitrary fixed to 0.5 and 0.33 arbitrary. Final polymer concentration is 0.1 wt%.*

Effect of the gadolinium to phosphate charge ratio on NP size, stability and relaxivity

Previous work on encapsulating hydrophobic salts in NPs via FNP showed that the charge ratio influenced NP loading and stability.[4] Thus, the effect of the charge ratio between the Gd^{3+} and PO_4^{3-} ions was investigated. The Gd^{3+} to PO_4^{3-} ratio was varied from 1/0.1 to 1/1.1 and the particle size and stability was evaluated. As shown in Figure S4a, NP size was constant at 30 nm up to a ratio of 1/0.75. Above the 1/0.75 ratio, large variations in size between samples were observed and the particles were unstable. We hypothesize that there is a critical number of lanthanide coordination sites necessary for the PAA-PEG polymer to anchor on the particle surface. Above the 1/0.75 ratio, there is an insufficient number of sites resulting in insufficient anchoring and thus poor particle stabilization.

We next investigated the effect of the charge ratio on the relaxivity properties of the stable samples. Because gadolinium must coordinated with water molecules to be MRI active, we hypothesized that as the PO_4^{3-} content is increased and displaces water molecules, the relaxivity would decrease. As shown in figure S4b., the r_1 and r_2 relaxivities of 30 nm particles decreases nearly 50% by increasing the Gd^{3+} to PO_4^{3} ratio from 1/0 to 1/0.75.

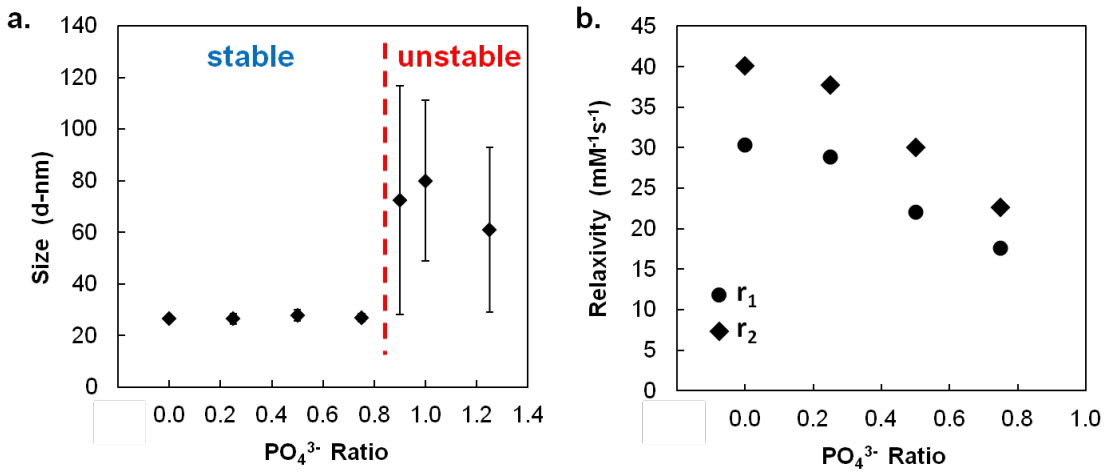

Figure S4. *(a) The effect of the Gd^{3+} to PO_4^{3-} ratio on NP size and stability. (b) The effect of the Gd^{3+} to PO_4^{3-} ratio on the relaxivity properties of 30 nm particles.*

Particle stability in storage conditions

In the manuscript, the particle stability over the course of 1 day determined *via* DLS is shown. The stability of $GdPO_4$ and $Gd_{0.5}Eu_{0.5}PO_4$ NPs stored at 4°C was additionally monitored up to six or eight days. The stability of a representative $GdPO_4$ MRI-only particle is shown in figure S5a. The particle size remains stable at 30 nm over the course of six days. The correlogram is also shown in figure S5b., indicating no change in the sample overtime. The stability of a representative $Gd_{0.5}Eu_{0.5}PO_4$ multi-modal particle is shown in figure S5c. The particle size remains stable at 40 nm over the course of six days. The correlogram is also shown in figure S5d., indicating no change in the sample overtime.

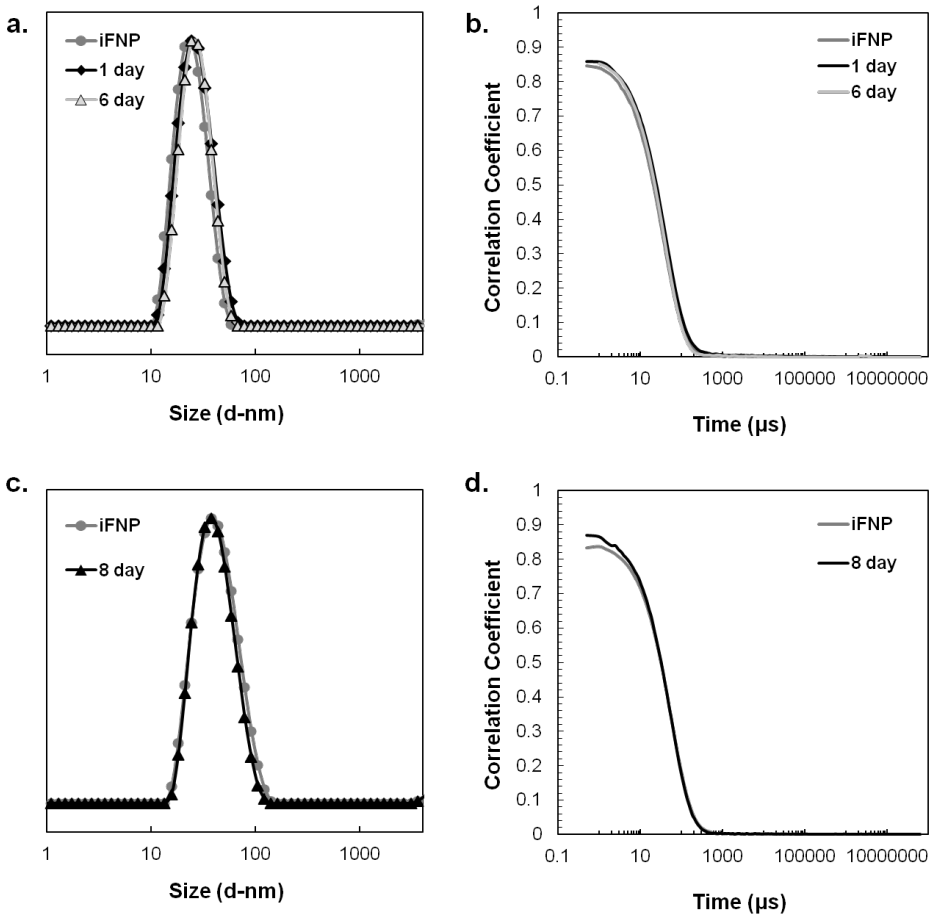

Figure S5. *(a) The intensity weighted particles size distribution of $GdPO_4$ NPs stored at 4°C overtime. (b) The correlogram of $GdPO_4$ NPs stored at 4°C overtime. (c) The intensity weighted particles size distribution of $Gd_{0.5}Eu_{0.5}PO_4$ NPs stored at 4°C overtime. (d) The correlogram of $Gd_{0.5}Eu_{0.5}PO_4$ NPs stored at 4°C overtime.*

Particle stability in biologically relevant conditions

For use in biological applications, NPs must be stable in biological media, which are rich in salts and protein. PEGylation is a common approach to confer stability to NPs in biological media. A dense PEG layer is known to minimize protein adsorption and subsequent aggregation. To test the stability of the PEGylated $GdPO_4$ and $Gd_{0.5}Eu_{0.5}PO_4$ NPs, particles were incubated in Tris-buffered saline (pH 7.4) with 3 wt% albumin at 37°C and monitored by eye and DLS for 24 hours. No precipitates were observed and the particle size remained constant over the course of 24 hours (Figure S6).

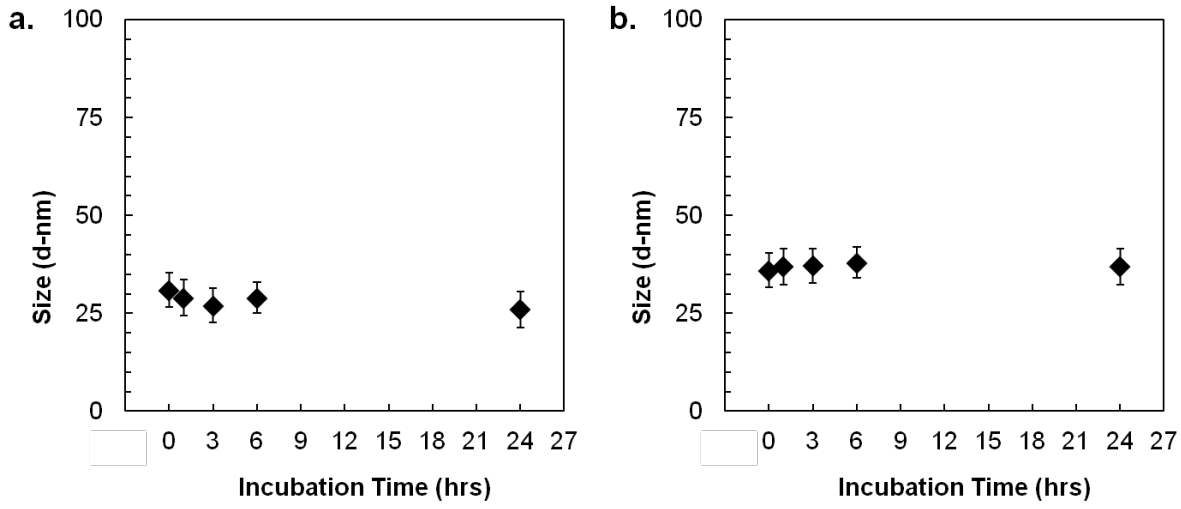

Figure S6. *The (a) $GdPO_4$ and (b) $Gd_{0.5}Eu_{0.5}PO_4$ nanoparticle size as a function of incubation time in biologically relevant media at 37°C is plotted.*

The intensity weighted size distribution plots of a buffered albumin solution and the $Gd_{0.5}Eu_{0.5}PO_4$ NPs solution prior to incubation is shown in Figure S7a. The albumin peak (7 nm) has minimal overlap with the $Gd_{0.5}Eu_{0.5}PO_4$ NPs peak (30 nm). The correlograms of the $Gd_{0.5}Eu_{0.5}PO_4$ NPs in albumin solution at 0 hour and after 24 hours of incubation are plotted in Figure S7b. The correlograms are identical, indicating minimal change in particle size distribution. Using the Malvern high resolution deconvolution mode, the albumin and $Gd_{0.5}Eu_{0.5}PO_4$ NPs peaks were resolved (Figure S7c). The albumin (10 nm) and $Gd_{0.5}Eu_{0.5}PO_4$ NPs NP peaks (40 nm) remain constant after 24 hours of incubation. Using the Malvern normal deconvolution mode, the peaks cannot be independently resolved (Figure S7d). Nevertheless the distribution does not change after 24 hours of incubation. This strongly suggests that the particles are stable in biologically relevant conditions.

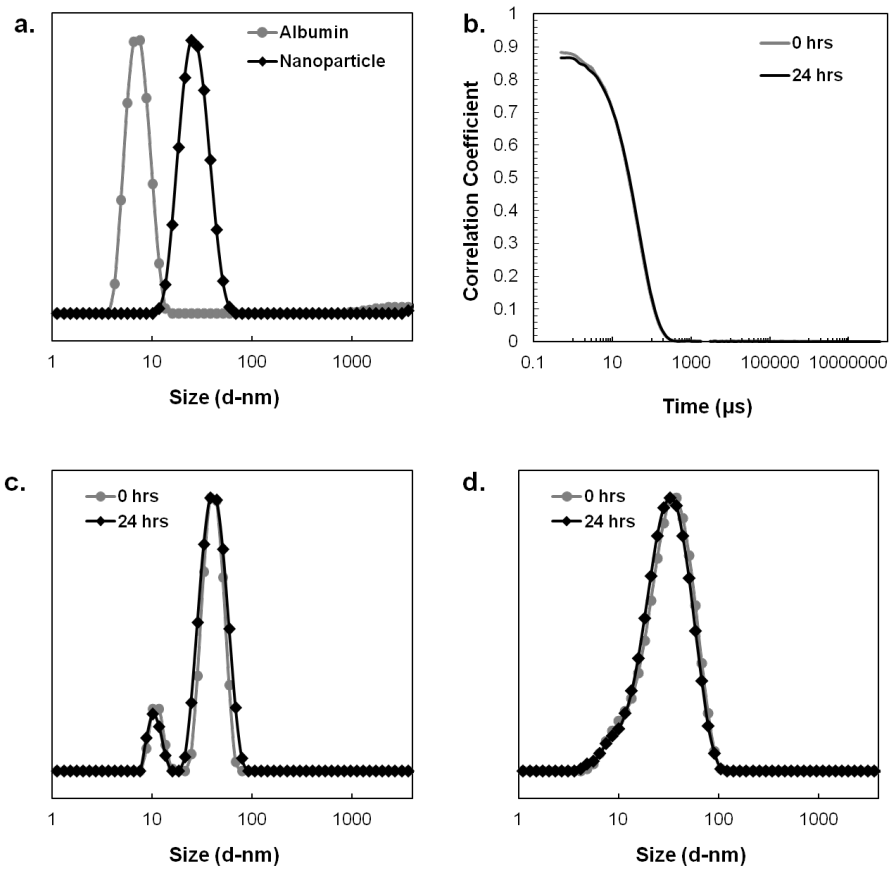

Figure S7. *(a) The intensity weighted size distribution plots of the albumin buffer solution and the $Gd_{0.5}Eu_{0.5}PO_4$ NPs solution (deconvolution: normal mode). (b) The correlograms, (c) the intensity weighted size distribution plots (deconvolution: high resolution mode) and (d) the intensity weighted size distribution plots (deconvolution: normal mode) of the $Gd_{0.5}Eu_{0.5}PO_4$ NPs in biologically relevant media at the 0 hr and 24 hrs time points.*

Effect of gadolinium to europium ratio on nanoparticle size

The Gd to Eu ratio does not appear to influence the NPs size within the sensitivity of the DLS. The intensity weighted size distributions and correlograms for NPs formed with a 1/0 Gd/Eu and a 0.5/0.5 Gd/Eu ratio is shown in Figure S8.

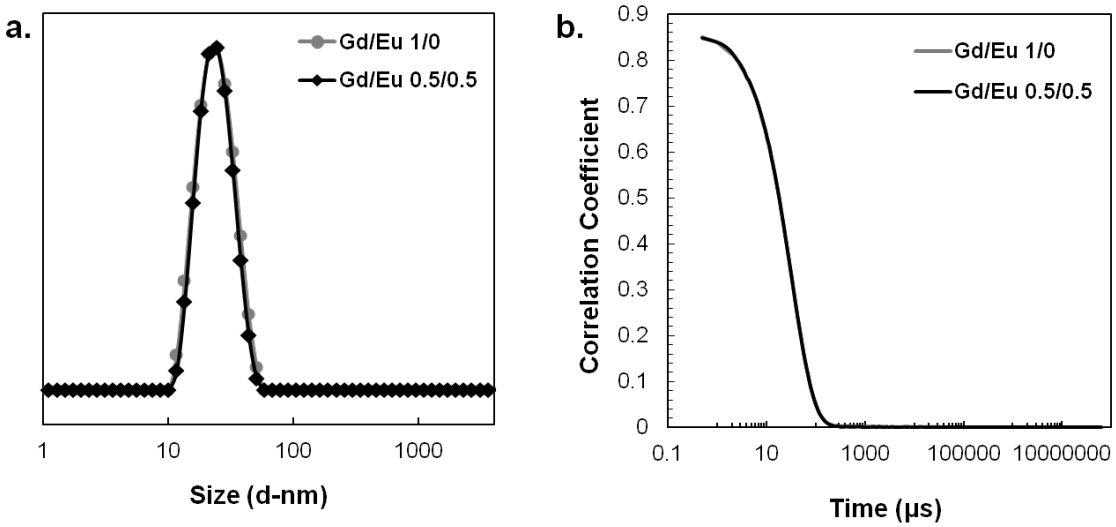

Figure S8. *(a) The intensity weighted size distribution of $GdPO_4$ and $Gd_{0.5}Eu_{0.5}PO_4$ NPs. (b) The correlograms of $GdPO_4$ and $Gd_{0.5}Eu_{0.5}PO_4$ NPs.*

Relaxivity

The r_2 to r_1 ratio as a function of the Eu to Gd ratio is shown in Figure S9. The ratio increases with Eu content.

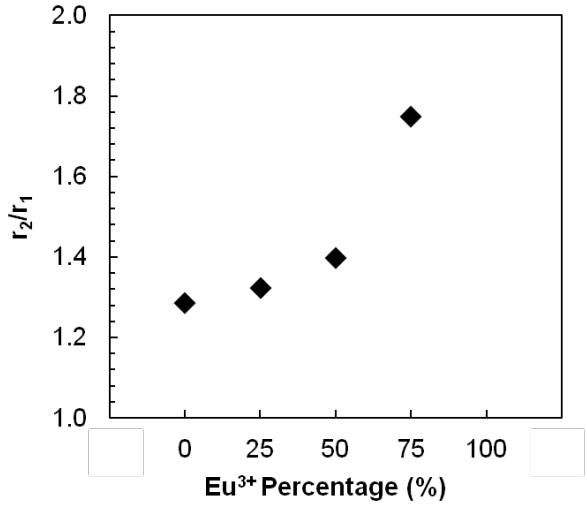

Figure S9. *The r_2 to r_1 ratio of $Gd_xEu_{1-x}PO_4$ NPs as a function of Gd to Eu ratio is plotted.*

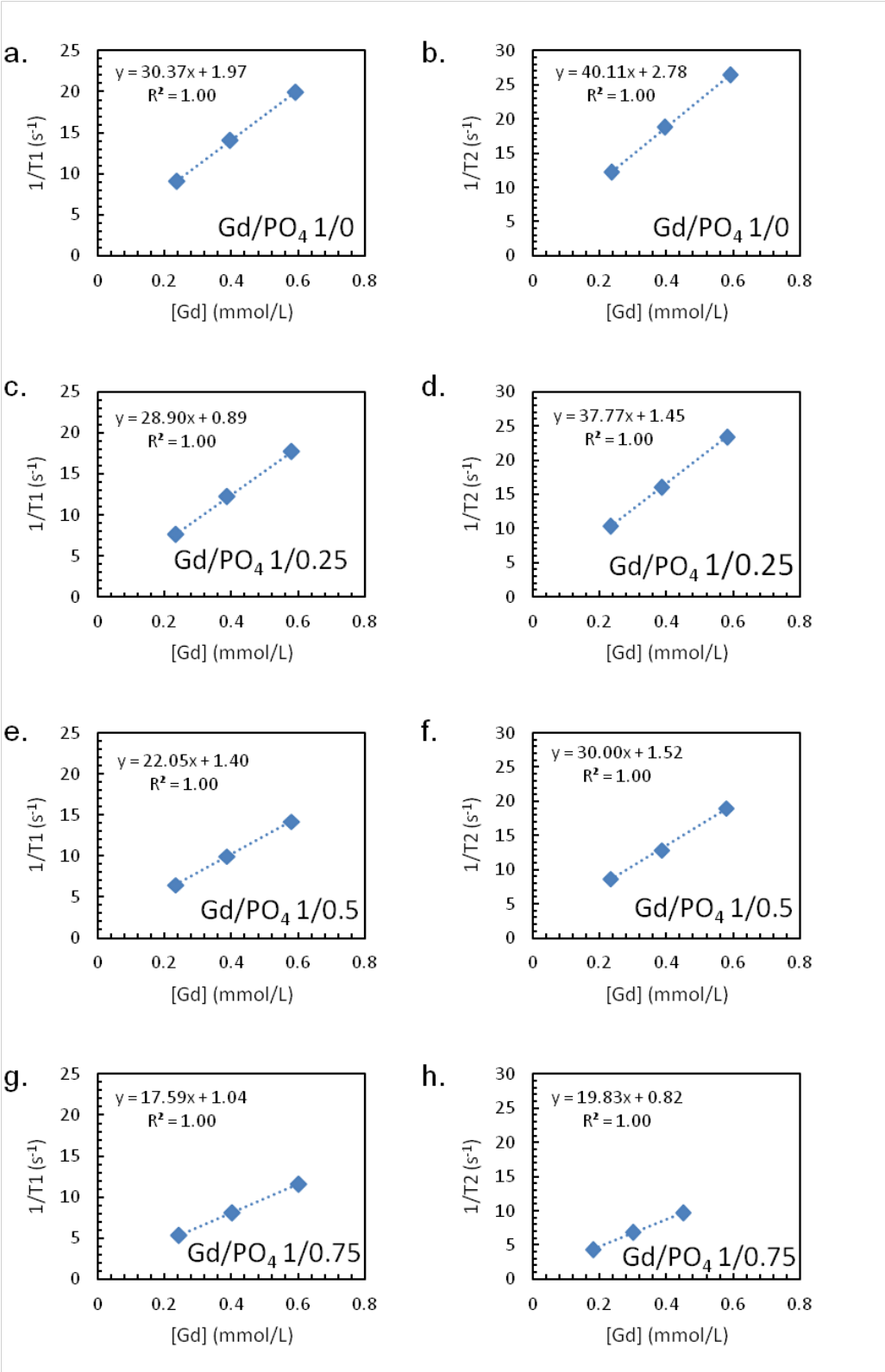

Figure S10. *Plots of T_1 relaxation rates (column 1) and T_2 relaxation rates (column 2) as a function of gadolinium concentration for $GdPO_4$ NPs with varying Gd to PO_4 ratios. (a-b) Gd/PO_4 1/0, (c-d) Gd/PO_4 1/0.25, (e-f) Gd/PO_4 1/0.5, (g-h) Gd/PO_4 1/0.75.*

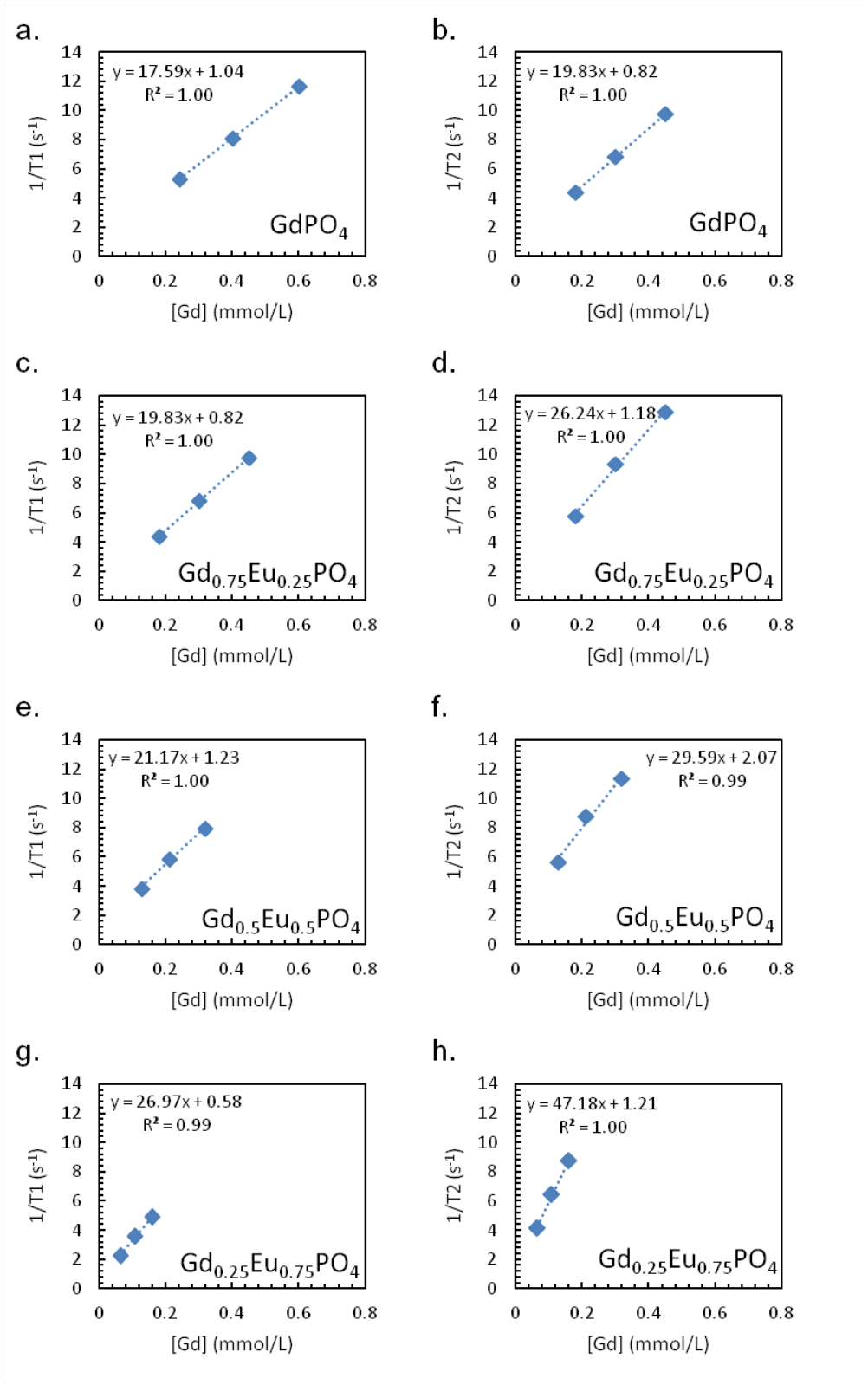

Figure S11. *Plots of T_1 relaxation rates (column 1) and T_2 relaxation rates (column 2) as a function of gadolinium concentration for $GdPO_4$ NPs with varying Gd to Eu ratios. (a-b) Gd/Eu 1/0, (c-d) Gd/Eu 0.75/0.5, (e-f) Gd/Eu 0.5/0.5 (g-h) Gd/Eu 0.25/0.75.*

XRD data

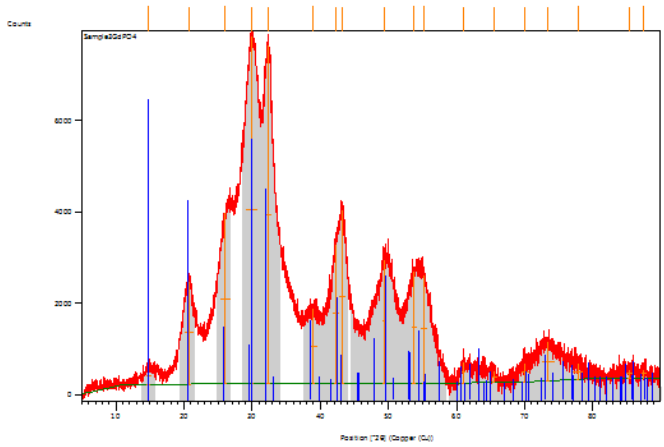

Figure S12. *The XRD trace of $GdPO_4$ salt formed without polymer via iFNP (red) is plotted with the peak pattern list for the $GdPO_4$ crystalline standard (blue). An overlap of all the major peaks is observed.*

Additional TEM images

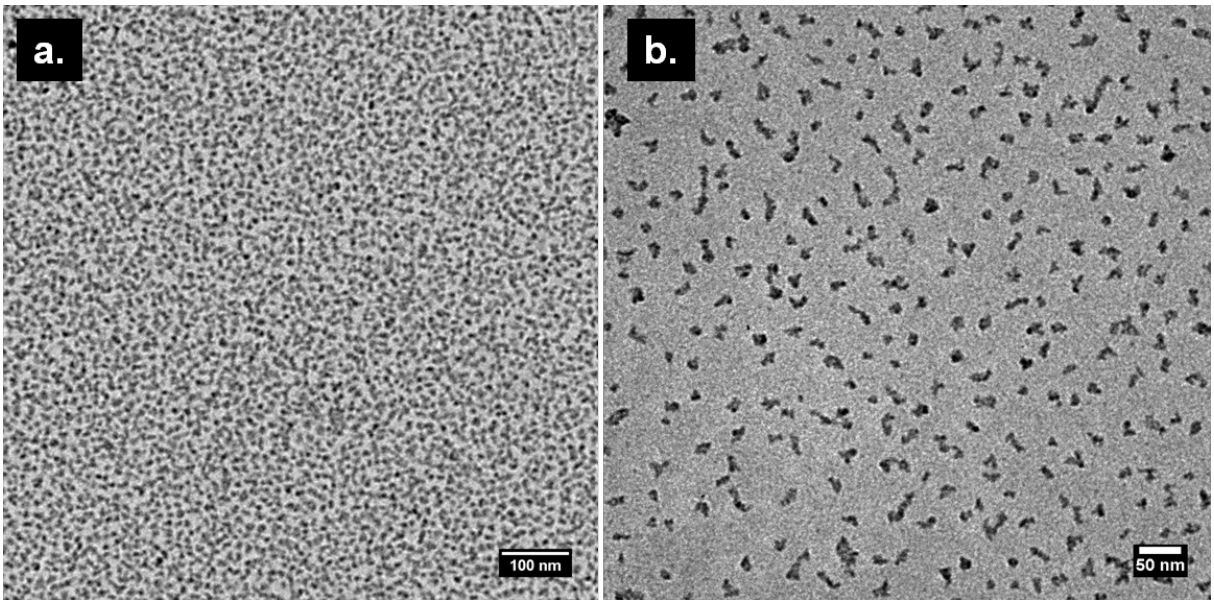

Figure S13. *TEM images of $GdPO_4$ NPs*

IndoCyanine Green (ICG) structure

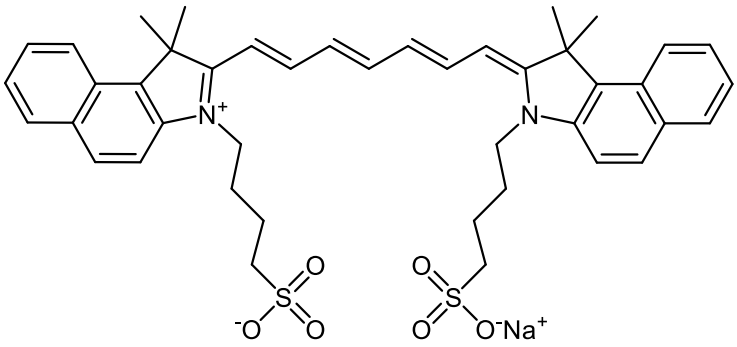

Figure S14. *The structure of the NIR-emitting fluorophore ICG, a water-soluble dye bearing two sulfonate groups able to interact with the $GdPO_4$ matrix.*

Additional *in vitro* images

Additional HeLa images are shown in Figure S15. A non-treated control can be found in Figures S15a-c, where no fluorescence signal is detected (Figure S15a). For the treated samples, a strong fluorescence is observable (Figures S15d,g,j). The overlaid fluorescence and bright-field images show a fluorescence signal localized around the cell nucleus. We hypothesize that the signal is coming from the Golgi complex.

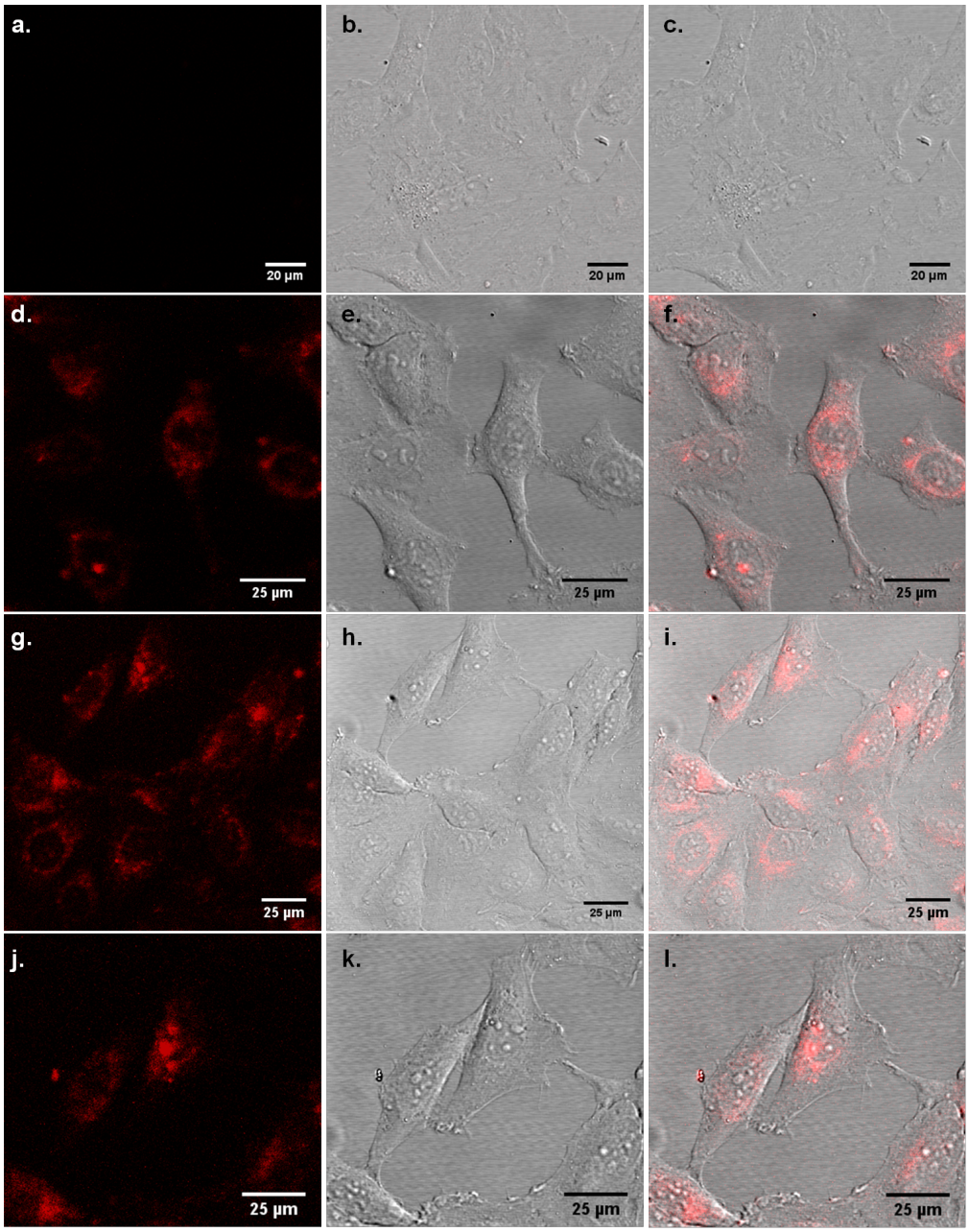

Figure S15. *The fluorescence signal (column 1), bright-field (column 2) and overlaid images (column 3) for non-treated control cells (a-c) and cells treated with $GdPO_4$•ICG nanoparticles for 3 hours (d-l).*

References

1. J. Han, Z. Zhu, H. Qian, A. R. Wohl, C. J. Beaman, T. R. Hoye, C. W. Macosko, *J. Pharm. Sci.* **2012**, *10*, 4018.

2. S. M. D'Addio, W. Saad, S. M. Ansell, J. J. Squiers, D. H. Adamson, M. Herrera-Alonso, A. R. Wohl, T. R. Hoye, C. W. Macosko, L. D. Mayer, C. Vauthier, R. K. Prud'homme, *JCR* **2012**, *1*, 208.

3. J. E. Gebhardt and D. W. Fuerstenau, *Colloids Surf.* **1983**, *1*, 221.

4. N. M. Pinkerton, A.Grandeury, A. Fisch, J. Brozio, B. U Riebesehl, R. K Prud'homme, *Mol. Pharm.* **2012,** 1, 319.